2023

Evaluating the relative influence of soil water potential, soil moisture, and vapor pressure deficit on semi-arid vegetation dynamics

Kayla R. Jamerson

EVALUATING THE RELATIVE INFLUENCE OF SOIL WATER POTENTIAL, SOIL MOISTURE, AND VAPOR PRESSURE DEFICIT ON SEMI-ARID VEGETATION DYNAMICS

By

KAYLA REBEKAH JAMERSON

Bachelor of Science in Geoscience, Fort Lewis College, Durango, CO, 2017

Thesis
presented in partial fulfillment of the requirements for the degree of

Master of Science
in Systems Ecology

The University of Montana
Missoula, MT

August 2023

Approved by:

Scott Whittenburg,
Graduate School Dean
Graduate School

Dr. Kelsey G. Jencso, Chair of Hydrology, Montana State Climatologist, Committee Chair
Montana Climate Office
W.A. Franke College of Forestry and Conservation

Dr. Zachary H. Hoylman
Montana Climate Office
W.A. Franke College of Forestry and Conservation

Dr. Anna Sala
Division of Biological Sciences

Dr. Ashley Ballantyne
Global Climate and Ecology Laboratory,
W.A. Franke College of Forestry and Conservation

Jamerson, Kayla, M.S., Summer 2023
Systems Ecology

Evaluating The Relative Influence of Soil Water Potential, Soil Moisture, and Vapor Pressure Deficit of Semi-Arid Vegetation Dynamics

Chairperson: Dr. Kelsey G. Jencsco

Knowledge of vegetation's response to soil water availability and atmospheric demand is critical to understanding the impact of climate change on semi-arid ecosystems. However, limited field-based research has been conducted to assess the relative importance of these drivers and previous research has simplified the assessment of soil water availability by relying on soil volumetric water content (VWC) as a primary control on plant growth, which, as opposed to soil water potential (Ψ_{soil}), does not account for the effects of soil texture on plant available water. To address these gaps, we compared remotely sensed indicators of vegetation response to field based measurements of VWC (at 20 cm depth), relative humidity and temperature (used to calculate the vapor pressure deficit, VPD) and soil temperature from 52 sites in Montana. Soil samples were collected at each site and were used to generate continuous time series of soil water potential (Ψ_{soil}). We utilized statistical analysis to assess the relationship of our biophysical metrics to satellite-derived estimates of vegetation health and vigor, including the Enhanced Vegetation Index (EVI), near-infrared reflectance vegetation index (NIRv), and solar-induced fluorescence (SIF). Results from this analysis suggest that Ψ_{soil} is a better biophysical indicator that VWC for driving seasonal vegetation productivity in semi-arid regions, while VPD emerges as a secondary driver in the absence of Ψ_{soil} limitations. Finally, anomalies in subsurface soil moisture were the dominant driver for explaining anomalies in vegetation response. These findings emphasize the importance of soil water potential as the first order control on vegetation water stress across semi-arid landscapes.

Table of Contents

1.0 Introduction

Droughts are projected to increase in frequency and intensity under warming climate scenarios across the globe (Cook et al., 2015; Dai, 2011; Xu et al., 2019). These prolonged periods of water limitation create adverse conditions in both the soil and atmosphere, affecting vegetation growth and productivity. Under these conditions, the combination of low soil moisture availability and high atmospheric water demand can induce stomatal closure in plants, limiting photosynthesis (Katul et al., 2012; Novick et al., 2016). This is particularly significant in semi-arid regions, which have been identified to be some of the most vulnerable ecosystems to drought impacts (Lian et al., 2021; Liu et al., 2018; Ma et al., 2015). Furthermore, these ecosystems comprise about 40% of Earth's land surface and are responsible for large contributions of interannual variability in global carbon sinks (Ahlstrom et al., 2015; Poulter et al., 2014). As climate continues to change, it is critical to understand the relative influences of atmospheric aridity and soil water limitations in regulating global carbon balance shifts in these vulnerable systems.

During photosynthesis plants open their stomata causing moisture loss from the plant in exchange for carbon dioxide; however, the mechanisms leading to stomatal closure remain uncertain and there currently remains a debate in the literature regarding the controls limiting plant growth during periods of prolonged water stress. High atmospheric aridity, often expressed as high vapor pressure deficits (VPD), can induce unfavorable hydraulic stress within plants, leading to stomatal closure as a preventative measure against excessive water loss to the atmosphere. Conversely, as soils dry, the reduced water uptake through plant roots can also induce stomatal closure. Cavitation in the plant xylem, which leads to hydraulic failure and wilting (Sperry et al., 2002), is caused both by excessive water loss and reduced soil water availability and stomatal closure can prevent cavitation in both cases. While both atmospheric demand and subsurface water supply are mechanistically linked to vegetation productivity dynamics, the relative importance of these contrasting controls remains unclear. Studies specifically focused on semi-arid or arid ecosystems at the regional scale have presented compelling evidence that soil moisture limitations play a dominant role in driving productivity (Xu et al., 2016; Yu et al., 2022). Additionally, other regional studies have found that the influence of VPD is heterogenous and can vary depending on vegetation type. For example, Wu and Gao (2021) assessed the interannual impacts of air temperature, VPD, and precipitation on vegetation growth for a semi-arid region in China and reported that none of these climatic factors had significant influence on vegetation productivity. They ultimately hypothesized that soil moisture was the main driver of vegetation productivity, without direct evidence. Other studies have reported that VPD limits the growth of Douglas fir (Restaino et al., 2016) or, conversely, that high VPD can increase photosynthesis in forested ecosystems (Green et al., 2020; Yu et al., 2022; Dubey and Gosh, 2023). However, there remains a shortage of research that has utilized field-based, in-situ observations to validate and strengthen these findings.

It is difficult to quantify the relative importance of the different drivers of vegetation response to water limitation due to the coupled relationship between soil moisture and atmospheric aridity (Novick et al., 2016). For example, during periods of water limitation, low soil moisture availability and high VPD frequently occur simultaneously due to land-atmosphere interactions (Zhou et al., 2019) making it difficult to disentangle their individual influences on vegetation growth. Additionally, high atmospheric aridity intensifies evapotranspiration rates from plants and the soil which can lead to subsequent declines in soil moisture over time (Zhou et al., 2019). Conversely, in the presence of sufficient soil moisture, high VPD can increase transpiration, which can enhance photosynthesis and promote productivity(Green et al., 2020), complicating empirical studies

Current research often simplifies plant response to soil water availability by focusing on soil moisture content (m^3/m^3; water per unit soil volume or mass), which is much easier to measure directly. This simplification neglects the influence of soil texture in determining plant access to soil water reservoirs, which may conceal the significance of soil water (Novick et al., 2022). For instance, as soils dry, soil water potential (Ψ_{soil}; kPa), which represents the tension by which soil water is bound to soil particles, becomes increasingly negative following highly non-linear relationships. Importantly, the same change in volumetric soil water content at the wet and dry extremes of the moisture continuum can result in substantially different changes in hydraulic stress on plants. Therefore, the physical properties of different soil types directly influence a plant's accessibility to water and the stress they experience. There is limited to no field-based research that has evaluated the role of Ψ_{soil} across regional ecosystems.

First principles suggest that Ψ_{soil} could be a more sensitive and precise biophysical indicator for assessing plant water stress than soil water content. This is because soil water tension is a more direct measurement of plant available water (Novick et al., 2022), regulating important processes, such as stomatal conductance (Jarvis, 1976) and the maintenance of photosynthesis (Boyer, 1970), that occur in both the soil and the plant. Water content transformations to Ψ_{soil} measurements are a required input in hydrologic equations and modeling, but Ψ_{soil} measurements are lacking across larger scales, due to the extensive amount of fieldwork and laboratory equipment required to relate water content to Ψ_{soil} (Novick et al., 2022). Models therefore must rely on Pedotransfer functions, which are empirical relationships that estimate soil hydraulic parameters from available soil data such as the soil texture and bulk density (Wösten et al., 2001). Novick et al. (2022) conducted a sensitivity analysis for the land-surface model ORCHIDEE and found that these estimated soil parameters from Pedotransfer functions are the main source of variability for Gross Primary Productivity (GPP) rates. This uncertainty limits our understanding and ability to predict ecosystem response to drought stress.

Despite our mechanistic understanding of how aridity in the soil and/or atmosphere can influence vegetation response, previous research focused on quantifying the relative importance of these different limiting drivers on vegetation growth has reported contrasting conclusions (Novick et al., 2016; Liu et al., 2020; Lu et al., 2022; Stocker et al., 2018; Yao et al., 2023; Yu et al., 2022; Yuan et al., 2019). The conflicting findings observed in the literature could be attributed, in part, to the wide variability in the methodologies and approaches employed across different studies. This variation spans from global assessments that utilize coarse spatial and temporal resolutions (Novick et al., 2016; Liu et al., 2020; Stocker et al., 2018; Yuan et al. 2019) to investigations focused on specific ecosystems at site level (Green et al., 2020; Yu et al. 2022). Furthermore, these studies have not incorporated field measurements of Ψ_{soil}, which is a more accurate and reliable variable than soil moisture. Finally, the prevalence of linear regression models in characterizing vegetation response to VPD and/or VWC (Novick et al., 2016; Liu et al., 2020; Stocker et al., 2018; Yu et al., 2022; Xu et al., 2016), despite the well-established understanding that these processes frequently exhibit nonlinear or threshold behavior (Daly and Porporato, 2005; Afshar and Yilmaz, 2017; Oddi et al., 2019), may also contribute to improper characterization. Consequently, the debate persists in the ecohydrologic literature regarding the relative significance of atmospheric water demand and subsurface moisture availability in determining vegetation productivity and vulnerability to drought.

Here, we address this gap in knowledge by investigating several key research questions: (1) which environmental drivers are most determinant for seasonal vegetation productivity dynamics in semi arid ecosystems? (1a) is Ψ_{soil} a better predictor of vegetation productivity than soil water content

(expressed as Volumetric Water Content, VWC (m^3/m^3))? (1b) are atmospheric or subsurface conditions more important for driving vegetation productivity? (2) are these drivers consistent when considering seasonal vegetation responses vs deviations from normal responses? To investigate these questions this study leveraged data from 52 sites in semi-arid climates across the state of Montana, with continuous measurements of environmental variables since 2016, including relative humidity and temperature (used to calculate VPD), VWC, and soil temperature. In addition to the field measurements, soil samples were collected at each site at 20 cm depth and laboratory analysis was conducted to calculate Ψ_{soil} and soil water retention curves were generated to back calculate field Ψ_{soil} from VWC. We utilized satellite imagery as a proxy for vegetation response and conducted statistical analysis utilizing generalized additive models (GAMs) to model and assess the vegetation productivity to these environmental variables.

2.0 Methods

2.1 Field Data

Study Site

The study area for this analysis was Montana, which is a headwater state located in the northwest continental United States. The climate of Montana is strongly influenced by the prevalence of the Continental Divide which results in precipitation and temperature differences for the west and east regions. West of the Continental Divide, the state is characterized by mountainous terrain that have a maritime climate of cooler summers and an average annual temperature of 39 F°. Western Montana receives more consistent precipitation relative to the eastern portion, with an average annual precipitation of about 22-30 inches. Eastern Montana generally consists of semi-arid continental climates that have warmer and drier summers with average annual temperatures of 44 F°. Eastern Montana generally receives limited, seasonal precipitation with an average annual precipitation of 12-14 inches. Statewide, the average annual temperature for Montana is 43 F° with summer temperature averages consistent of 64 F° and the average annual precipitation is about 18.7 inches.

Environmental data was collected at Montana Mesonet stations, a network of 95 weather and soil moisture stations distributed across the state of Montana (Figure 1). Each of the sites have been continuously measuring these environmental variables since 2016 and they have recorded periods of water surplus and deficit. The majority of the Montana Mesonet stations are predominantly covered by perennial forbs and grasses, followed by annual forbs and grasses, litter, bare ground, and shrubs (Figure S1).

Montana Mesonet Data

At each of the Montana Mesonet stations, relative humidity and temperature (to calculate VPD), VWC and soil temperature were collected at a 10-minute interval. Relative humidity and temperature were measured at 2-meter height above ground and soil moisture and soil temperature was recorded at 10 cm, 20 cm, 50 cm, and 100 cm soil depths. Soil temperature was also included in this analysis because it impacts important biological and chemical processes that directly influence water and nutrient uptake (Hillel, 2003; Kasper and Bland, 1992). Soil samples were collected at 52 stations (Figure 1), where Ψ_{soil} was computed for the 20 cm depth using laboratory procedures (below). The data was grouped by individual sites from which we calculated weekly averages of each of the environmental variables.

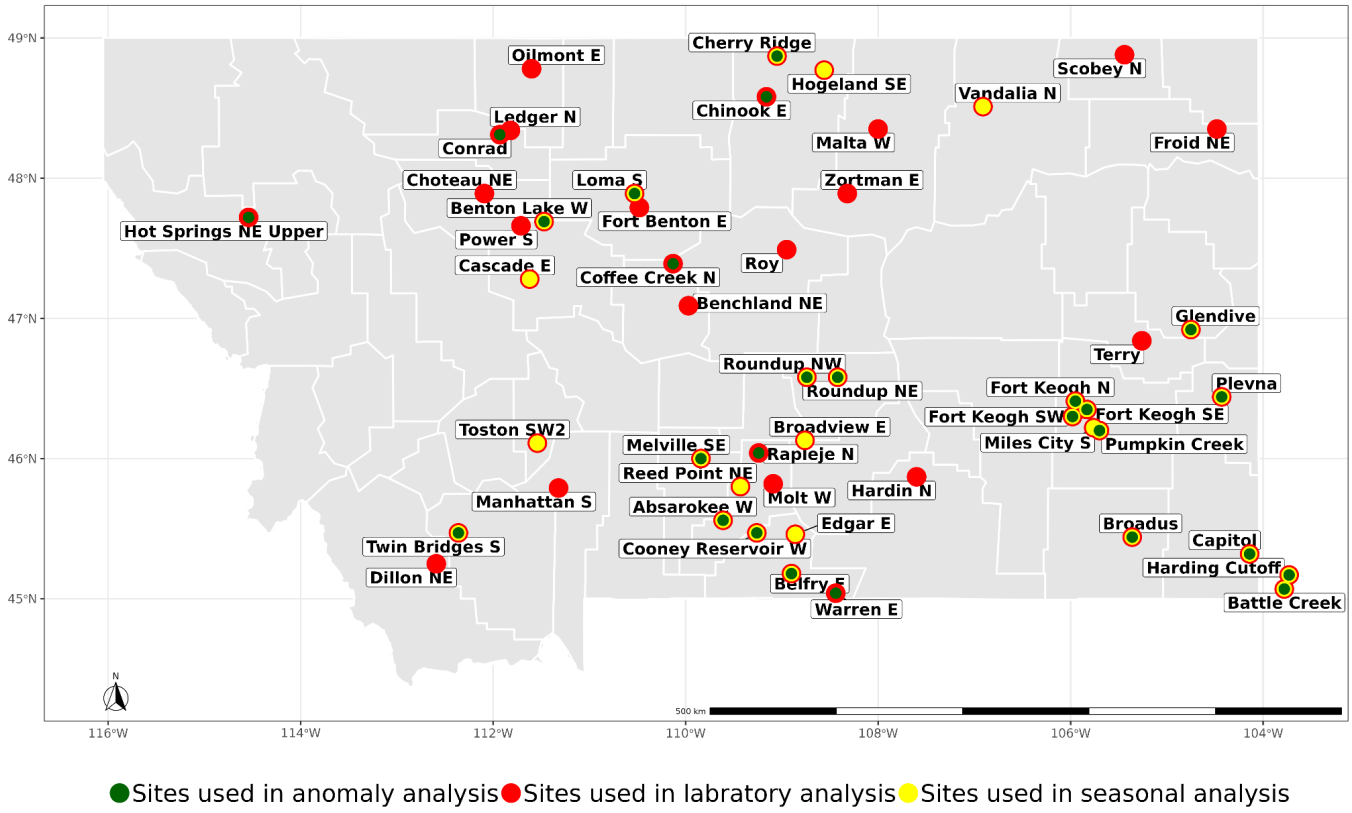

Figure 1. The spatial distribution of 52 of the Montana Climate Office Mesonet stations across the state of Montana. Locations where soil samples were collected to generate the Ψ_{soil} measurements are indicated by red symbols. Sites included in the seasonal analysis are indicated by yellow symbols (28 stations), while sites included in the anomaly analysis are indicated by green symbols (26 stations).

2.2 Laboratory Procedures

We developed soil water retention curves (SWRC, e.g. the relationship between VWC and Ψ_{soil}) in the laboratory in order to generate time series of Ψ_{soil}. Ψ_{soil} measurements were obtained using Hydraulic Property Analyser (HYPROP) and the WP4C instrument (METER Group, 2019). The HYPROP uses two tensiometers of different lengths to measure water potential in the wet range of the SWRC (approximately 0.20 to 0.45 m^3/m^3VWC; Figure 2). These tensiometers can measure water potential up to the air entry point, which corresponds to the atmospheric pressure at about 100 kPa where water begins to vaporize. The dry end of the SWRC, beyond the sensitivity of the in-situ tensiometers, is obtained using the WP4C instrument (as shown by the 4 measurements above 0.20 m^3/m^3 in Figure 2). The WP4C is capable of

measuring exceptionally dry ranges, up to 300000 kPa. The combination of the HYPROP and WP4C provides a full range of Ψ_{soil} measurement for various stages of water content ranging from field capacity (0 to 100 kPa) to exceptionally dry (100 to 300 mPa) (Figure 2).

Soil Water Retention Curves

Numerous studies have focused on developing SWRC to accurately describe the highly nonlinear relationship between water content and Ψ_{soil}. The earliest and most widely recognized models were proposed by Brooks and Corey (1964) and van Genuchten (1980). These empirical equations are based on the concept of cylindrical capillaries and effectively predict the wet end of the SWRC, ranging from saturation to residual water content (Leong et al., 1997). However, they assume infinite matric suction for water content below the residual water content, thus failing to capture the dry end of the SWRC with precision (Corneilis et al., 2005). Nonetheless, these models continue to be extensively utilized within the soil physics community (Russo, 1988; Fuentes et al., 1992; Stankovich and Lockington, 1995; Ghanbarian-Alavijeh et al., 2010; Soto et al., 2017). Subsequent models have been developed in an effort to better predict the full range of the SWRC, spanning from saturation to oven-dryness, by considering the relationship between the retention curve and the soil pore size distribution (Zheng et al., 2020). Noteworthy models include the one proposed by Fredlund Xing (1994), which incorporates the soil-size distribution function to determine the curve shape, and the model developed by Kosugi (1999), who applies a lognormal distribution function to the soil pore radius distribution. We utilized four widely recognized and extensively used SWRC: the Brooks and Corey (BC), the van Genuchten (VG), the Kosugi (K) , and the Fredlund and Xing (FX) models, summarized in Table 1. These models were chosen based on their prominence and frequent application in the field of soil science (Soto et al., 2017; Too et al., 2014; Too et al., 2021; Zheng et al., 2020).

The BC, VG, K, and FX models were fit to the measured SWRC, developed from laboratory procedures, for each site. We then calculated the Mean Standard Error (MSE) for each model and used this measure of error to select the best-fit model with the lowest MSE. Model fitting and data analysis was performed using the R programming environment (R Core Team, 2020). Each SWRC was computed using non-linear regression analysis, specifically, the nlsLM R package (Elzhov et al., 2010).

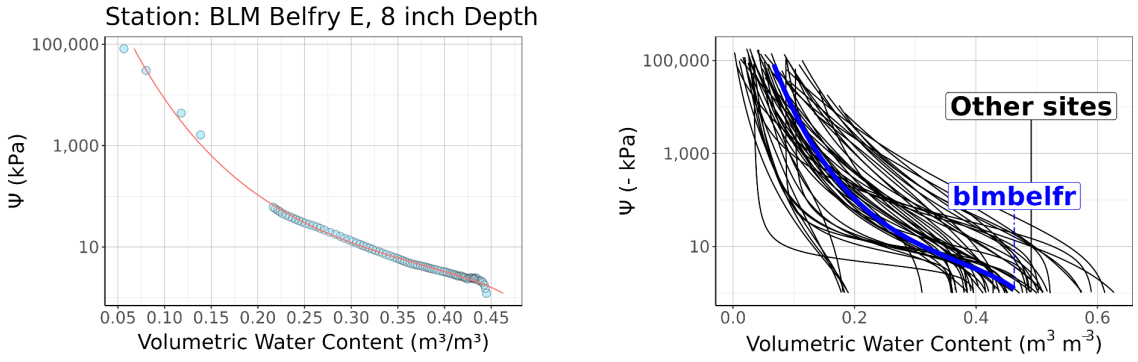

Figure 2. SWRCs generated for 20 cm depths across all sites illustrate the influence of soil texture on soil moisture availability.

The nlsLM package uses the Levenberg-Marquardt algorithm (Levenberg, 1994; Marquardt, 1963) to solve the nonlinear least square problems and determines appropriate parameters by running a series of iterations. The SWRC generated for each site was subsequently used to inversely model a time series of Ψ_{soil}.

Table 1. Summary of Soil Water Retention Curves (SWRC) considered in this analysis.

SWRC	Equation	Authors
BC	$\Theta = \Theta_r + \left(\Theta_s - \Theta_r\right)\left(\frac{\Psi}{\alpha}\right)^{-\lambda}$ Where Θ is volumetric water content (VWC), Θ_s is saturated water content, Θ_r is residual water content, Ψ is the soil matric potential, α is the air-entry value, and λ is the pore size distribution of the soil.	Brooks and Corey (1964)
VG	$\Theta = \Theta_r + \left[\frac{\Theta_s - \Theta_r}{1+\alpha\psi^{\lambda}}\right]^{\left(1-\frac{1}{\lambda}\right)}$	van Genuchten (1980)
K	$\Theta = \Theta_r + 0.5\left(\Theta_s - \Theta_r\right) erfc\left[ln\left(\frac{\frac{\psi}{\phi}}{\sqrt{2}\sigma}\right)\right]$ Where ϕ is the geometric mean of the pore capillary pressure distribution function and σ is the standard deviation of the pore capillary pressure distribution function.	Kosugi (1999)
FX	$\Theta = \Theta_r + \frac{\left(\Theta_s - \Theta_r\right)}{ln\left(e + \left(\frac{\Psi}{h}\right)^n\right)^m}$ Where *h*, *n*, *m* are shape fitting parameters.	Fredlund Xing (1999)

2.3 Vegetation Response Datasets

Satellite based observations of vegetation reflectance and emittance serve as valuable tools for evaluating vegetation productivity at regional and global scales. When choosing appropriate vegetation indices for this analysis we leveraged the work of Wang et al. (2022), who compared various satellite-based measurements with eddy-covariance flux tower estimates of gross primary productivity (GPP) in semi-arid and arid ecosystems. This study found that the near-infrared reflectance vegetation index (NIRv) and Solar Induced Fluorescence (SIF) performed the best in capturing seasonal GPP variations. NIRv was particularly effective for low-productivity ecosystems, while SIF showed stronger correlations with high-productivity ecosystems such as evergreen forests. NIRv combines the Normalized Difference Vegetation Index (NDVI, a measure of the difference between near-infrared (NIR) light and

red light), with the fraction of NIR reflected by vegetation. NIRv takes into account canopy structure and effectively reduces noise associated with soil brightness (Badgley et al., 2017). NIRv is calculated as:

$$NIRv = (NDVI - 0.08) * NIR;\ NDVI = \frac{NIR - R}{NIR + R}, \quad (1)$$

where NIR is the near-infrared band (770 - 800nm) and R is the red band (630 - 760nm). SIF is an alternative satellite-based measurement of vegetation produtivity dynamics. Unlike NIRv, SIF is not a measure of greenness; instead it quantifies the solar radiance emitted from chlorophyll molecules during photosynthesis activities. SIF is calculated as:

$$SIF = PAR * FPAR * \Phi_F * f_{esc}$$

where PAR is the incoming photosynthetically active radiation, FPAR is the fraction of PAR absorbed by chlorophyll, Φ_F is the quantum emission yield of SIF, which is the ratio of emitted to absorbed photons for the canopy and f_{esc} is the fraction of SIF photons that escape from the canopy. Another commonly used vegetation response metric is the Enhanced Vegetation Index (EVI), which is a reflectance-based indicator of vegetation greenness commonly used to estimate vegetation growth, health, and vigor (Huete et al., 1999). EVI is a modified version of NDVI but includes the blue band to mitigate noise associated with dense vegetation and atmospheric influences. EVI is calculated as:

$$EVI = 2.5\left(\frac{NIR - R}{NIR + 6*R - 7.5*B + 1}\right)$$

where B is the blue band (459-479nm).

In this study, we used EVI, NIRv, and SIF observations as proxies for vegetation response. EVI and NIRv were extracted from the MODIS satellite using Google Earth Engine (Gorelick et al., 2017). When available (e.g. NIRv), we utilized a quality assurance (QA) layer, and filtered for time periods with only high quality data. SIF data was extracted from the dataset published by Hu et al. (2022), who generated seamless global daily SIF products at a 0.05-degree resolution from May 2018 to December 2020. This SIF dataset was generated using the random forest approach with inputs from TROPOspheric Monitoring Instrument (TROPOMI) SIF, MODIS reflectance data, and meteorological data from ERA5.

2.4 Statistical Analysis

The empirical analysis can be further divided into two components: seasonal analysis and anomaly analysis (Figure 1). In the seasonal analysis, we investigate the relative importance of environmental drivers for predicting seasonal vegetation productivity dynamics, for the years of 2016 to 2022. We aggregated the data by conditions across the entire state of Montana and assed the independent effects of our predictor variables on vegetation response. Additionally, we evaluated the combined effect of the predictor effects and aggregated the data by individual sites. In the anomaly analysis, we aimed to identify the drivers that account for deviations from the normal vegetation response.

All data was filtered for the growing season from May 1st through September 30th. To ensure accurate Ψ_{soil} data, sites with a SWRC Mean Standard Error (MSE). Lastly, the value exceeding 0.00015

was excluded. This threshold was determined by evaluating the distribution of error associated with the SWRC best fit models (Figure 4). These anomalously erroneous models were likely attributed to methodological errors in field or laboratory procedures (refer to Figure 4 in the results section for a distribution of MSE values for all SWRCs).

2.4.1 Seasonal Analysis

To evaluate the relative influence of our explanatory variables (Ψ_{soil}, VWC, VPD, and soil temperature) on vegetation productivity (EVI, NIRv, and SIF), we used Generalized Additive Models (GAMs). GAMs utilize non-parametric smoothing functions on predictor variables, allowing for approximation of non-linear effects commonly observed in ecological data. To do so, we utilized the GAM function from the mgcv R package (Wood, 2012) assuming a Gamma distribution and a log link function. A Gamma distribution was used to model our response datasets (EVI, NIRv and SIF) because they are functionally bound between 0 and infinity. To address issues of overfitting and model complexity, the smoothing functions were limited to 6 degrees of freedom. Furthermore, a square root transformation was applied to the Ψ_{soil} values, as the raw data spanned several orders of magnitude. By applying this transformation, the data was brought to a more comparable scale and facilitated a meaningful analysis across the wide range of Ψ_{soil} values.

In order to determine relative variable importance in describing vegetation dynamics, we calculated the partial deviance change (PDC) of each predictor associated with each GAM model. This approach is similar to methods described by Brunbjerg et al. (2018), and begins by fitting a full GAM model that includes all predictor variables and calculating the model deviance. Subsequently, we constructed an alternative model by excluding the predictor variable of interest from the full model, while keeping the smoothing parameters and dispersion parameters fixed. The new, alternative model deviance is then recalculated. The difference between the deviance from the full model and the alternative model with the dropped term represents the PDC for that particular predictor variable. A higher PDC score indicates that the predictor variable explains a greater amount of deviance, suggesting its higher importance as a predictor. It is important to note that the PDC values will not sum up to 100% due the non-orthogonal nature and nonlinear relationships and interactions that are inherent in GAM models. However, the PDC provides valuable insights into the relative importance of predictor variables compared to others used in the model.

Dominant vegetation type was also considered in site selection for the seasonal analysis, in order to ensure consistency in the relative magnitude of our vegetation indices (EVI, NIRv, and SIF) across sites. This filtering allows us to focus on capturing differences in vegetation conditions in response to environmental factors rather than variations in vegetation index values related to differences in vegetation types. To do so, we utilized 30m vegetation cover products from the Rangeland Analysis Platform (RAP) to extract vegetation class information for all years (Allred et al., 2021; Jones et al., 2018). RAP provides annual estimates of perennial forbs and grasses, annual forbs and grasses, shrubs, bare ground, litter and trees. We calculated dominant vegetation cover for each station by extracting annual percent cover estimates from 2017 to 2022. The dominant vegetation class and sub-dominant (second most abundant) vegetation class were then computed from these data. Dominant and sub-dominant vegetation classes were only used if they accounted for 50% or more of the total vegetation class distribution (e.g. 35% perennial forbs and grasses and 25% annual forbs and grasses) of the 30-meter area at a station. The dominant vegetation cover was perennial forbs and grasses, followed by the sub-dominant vegetation covers of annual forbs and grasses, litter, bare ground, and shrubs. The majority of the Montana Mesonet

stations were predominantly covered by perennial forbs and grasses (Figure S1). Sites that had a different dominant and sub-dominant vegetation cover than those shown in Figure S1, or no dominant cover, were excluded from the analysis. After applying these filters, the final dataset for the seasonal analysis consisted of 28 sites (see Figure 1).

To discern the individual effects of environmental drivers on vegetation, we aggregated vegetation response by condition (e.g. similar subsurface or atmospheric conditions), in addition to the previous method of focusing on individual sites. This analysis helped to evaluate variance in NIRv responses across conditions and how strongly individual environmental variables drive vegetation productivity. We utilized data binning, where the range of each predictor variable was divided into equal bins along its distribution. For each bin, the median value was calculated to quantify the median NIRv, along its upper and lower interquartile range.

2.4.2 Anomaly Analysis

The seasonal analysis yields valuable information on predictor importance; however, it does not disentangle the natural seasonal decline in vegetation productivity that is commonly observed at the onset of fall, from differences observed in high productivity or low productivity years (Figure 3). Calculating standardized anomalies allow us to assess variation across NIRv and to examine if anomalies in the environmental drivers explain deviations from normal vegetation responses. This is similar to a "z-score", in which the data is normalized by the mean conditions. We conducted a 31-day moving window analysis for each day across all years, which considers the values 15 days before and 15 days after day *i* and builds a probability distribution function (PDF). A PDF fits a gamma distribution (with the exception of the soil temperature dataset, which uses a generalized logistic distribution due to its ability to handle negative values) to the dataset within the 31 day window. The center of the resulting PDF are the average or expected conditions for day *i* and deviations from the mean are anomalies (relative to the mean of the PDF). We applied this method for each predictor variable, as well as NIRv, to generate a new dataset specifically focused on anomalies. We selected sites that had a minimum of at least 3 years of data (2018 - 2021). Vegetation cover was not considered in the anomaly analysis because it accounts for differences in absolute magnitudes from the spectral indices. The methodology described in the seasonal analysis was then replicated for the anomaly data, and a full GAM model was fitted using all predictor anomalies and the NIRv anomalies. We again calculated a PDC to determine the importance of each predictor in explaining the observed anomalies.

3.0 Results

3.1 Laboratory Analysis

The FX, VG, K and BC functions were fit to the soil water retention data from 52 sites at the 20 cm depth, with the selection based on the lowest mean squared error (MSE) value. Among the tested functions, the FX model was the best fit for the majority of the sites (37 sites), followed by the van Genuchten model (13 sites) and the Kosugi model (2 sites), while the BC model did not provide the optimal fit for any of the sites (refer to Figure 4). To ensure data quality (e.g. the transformation function from VWC to Ψ_{soil} was accurate), four sites were excluded from the analysis due to an MSE value exceeding the threshold of 0.00015.

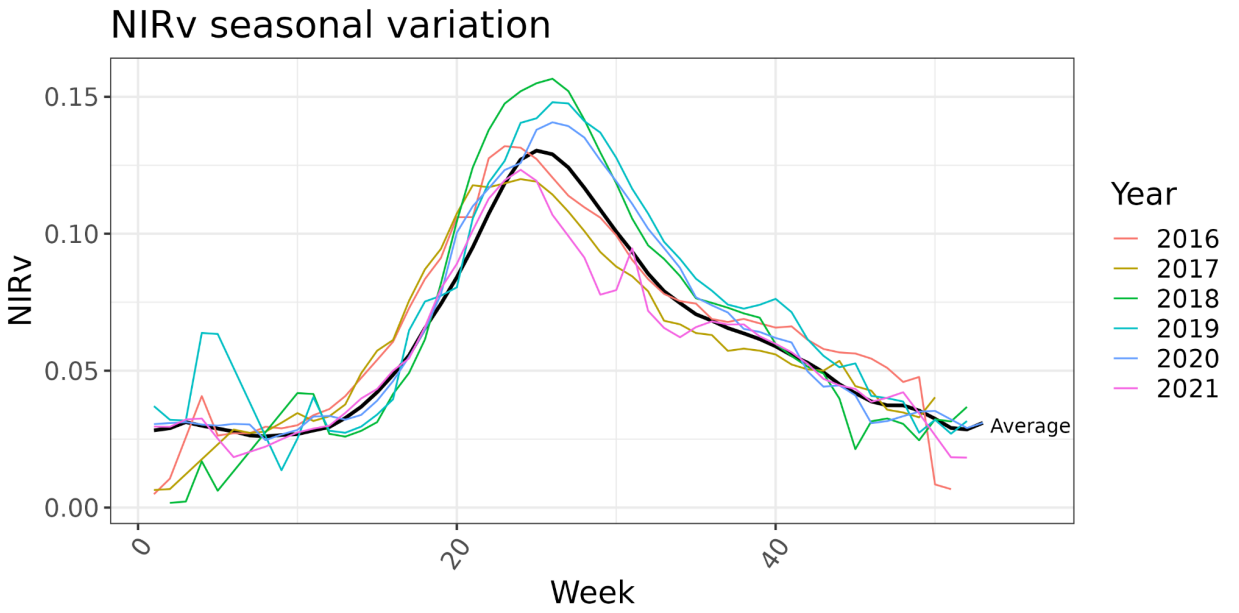

Figure 3. Anomalies calculated using a 31-day moving window reveal the predictors responsible for deviations from the average seasonal response across all sites (shown in graph above), exemplified by the contrasting productivity between 2018 and 2021.

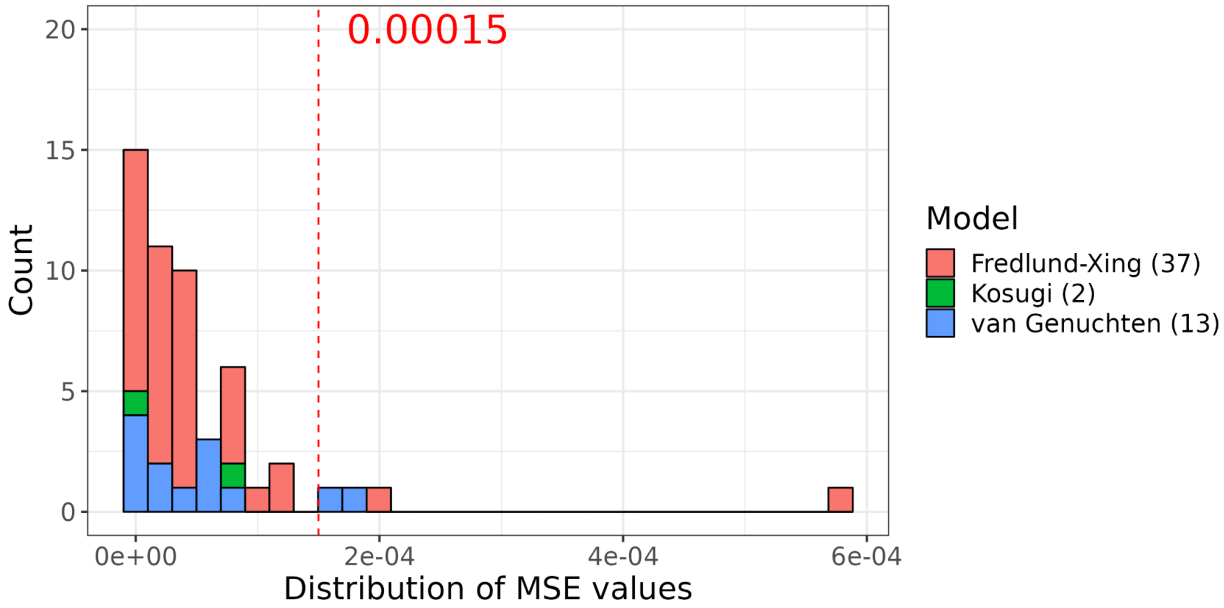

Figure 4. Distribution of Mean Standard Error (MSE) values from the Soil Water Retention Curves (SWRCs).

3.2 Seasonal Analysis

We modeled site specific vegetation responses to seasonal variations in subsurface and atmospheric conditions using three GAM models. The summary outputs for each GAM model for NIRv, EVI and SIF are presented in Table 2. All GAM models exhibited a similar degree of deviance explained, ranging from 20.14% to 24.93%. The adjusted R-Squared values were 0.192 for NIRv, 0.173 for EVI, and 0.192 for SIF. Notably, Ψ_{soil} demonstrated the highest PDC value across all models, indicating that Ψ_{soil} is a dominant driver of vegetation productivity (Table 2). However, the ranking of the PDC values for the remaining predictors varied depending on the vegetation index. Following Ψ_{soil}, VPD displayed relatively high PDC values, ranking as the second-highest predictor in the NIRv and SIF models, and the third-highest predictor in the EVI model. VWC and soil temperature consistently showed lower PDC values across all models, with the exception of VWC for the EVI model, which ranked second.

Model	Variables	Partial Deviance Change	edf	Ref.df	F	p-value	Deviance Explained
NIRv	**Ψ (sqrt kPa)**	**79.85806**	**4.165135**	**4.694610**	**38.5150271**	**0.0000000**	**20.14%**
NIRv	VPD (kPa)	51.39041	1.000312	1.000614	55.2871938	0.0000000	20.14%
NIRv	VWC (m³/m³)	41.61939	4.811321	4.981420	10.1779136	0.0000000	20.14%
NIRv	Soil Temperature (C)	33.79366	2.825420	3.480443	8.5397783	0.0000070	20.14%
EVI	**Ψ (sqrt kPa)**	**31.99457**	**4.622528**	**4.932055**	**32.4477619**	**0.0000000**	**24.54%**
EVI	VWC (m³/m³)	14.00974	4.863618	4.990199	10.5848781	0.0000000	24.54%
EVI	VPD (kPa)	13.34396	4.480736	4.882598	14.0193116	0.0000000	24.54%
EVI	Soil Temperature (C)	6.19825	4.390827	4.833713	3.4289631	0.0050501	24.54%
SIF	**Ψ (sqrt kPa)**	**188.77658**	**4.655427**	**4.939424**	**63.4836772**	**0.0000000**	**24.93%**
SIF	VPD (kPa)	84.49327	4.159311	4.711645	10.5989421	0.0000000	24.93%
SIF	Soil Temperature (C)	69.85566	2.405973	3.033341	18.1748029	0.0000000	24.93%
SIF	VWC (m³/m³)	45.14176	1.000549	1.001095	0.0009872	0.9825143	24.93%

Table 2. Overview of GAM model summary outputs and PDC for NIRv, EVI, and SIF.

The partial effect plots of each predictor variable in the GAM models are presented in Figure 5. Increase in EVI, NIRv and SIF all indicate more productive ecosystems, referred to here as vegetation productivity. Across all models, both Ψ_{soil} and VPD have a negative effect on productivity, where vegetation productivity tends to decrease with increasing dryness. A threshold was observed for Ψ_{soil} at approximately 400 kPa, beyond which vegetation productivity exhibits a steeper decline. The SIF and EVI GAM models revealed an additional pattern with respect to atmospheric dryness; vegetation productivity is associated with increased VPD up until roughly 1 kPa, after which we observed a generally negative effect. Soil temperature had a consistent, positive effect, with increases in vegetation productivity associated with rising temperature. VWC exhibited inconsistent effects on vegetation productivity. There is an exception for SIF, where VWC displayed no significant effect. Figure 6 shows

the model predictions when using all predictor variables within the GAM models. The productive (i.e. wet/green) end of the vegetation indices reveal increased variability and dispersion between the observed and predicted values. Conversely, the unproductive (i.e. dry/brown) end of the vegetation indices demonstrated better model performance.

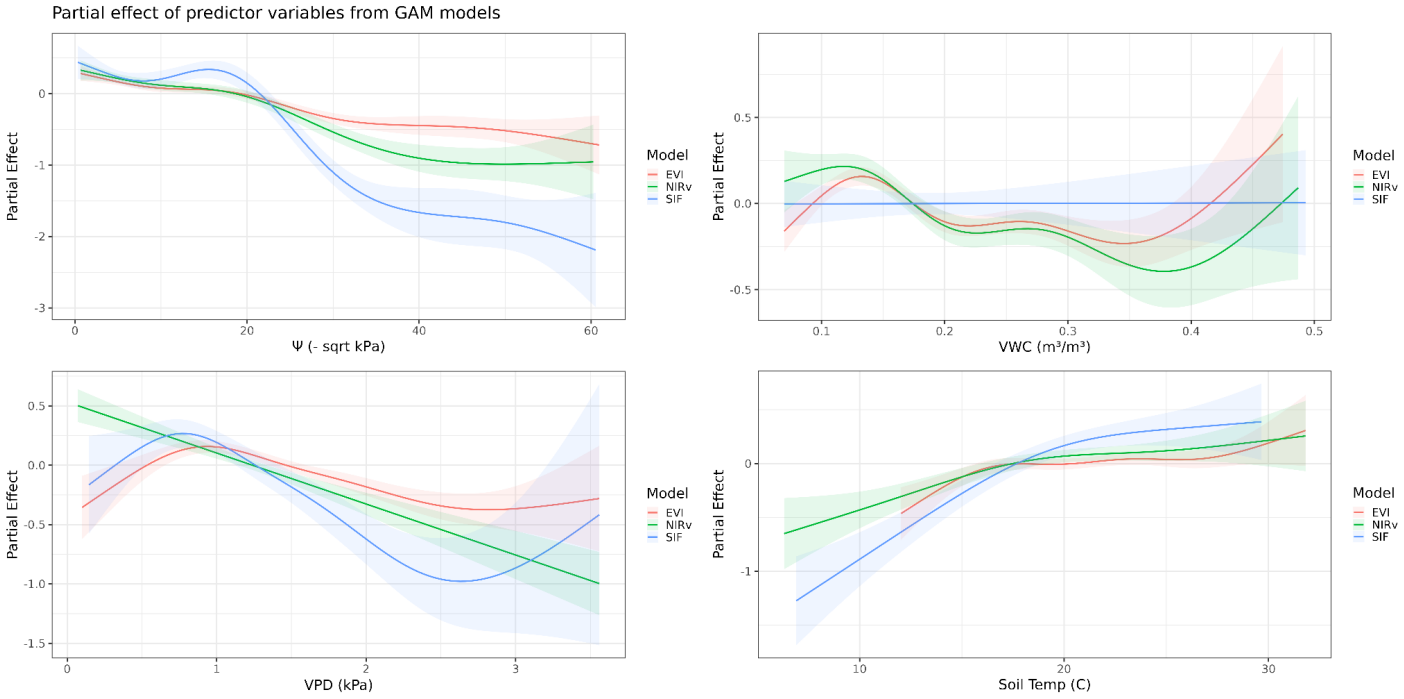

Figure 5. Partial effect functions for each predictor variable in the GAM models. Partial effect plots show how the response variable changes with changing conditions from a predictor variable of interest, while holding all other predictor variables in the model at a constant average.

NIRv was aggregated across Montana for each predictor variable (e.g. all sites were aggregated and vegetation response was binned according to predictor variables) to assess the independent effects of each environmental variable on vegetation response (Figure 7). We exclusively utilized NIRv as the chosen satellite index for this step (as well as the anomaly analysis), due to the limitations of having less data available from the SIF and EVI datasets. Using NIRv is also supported by the findings from Wang et al. (2022) that identified NIRv to be the most suitable proxy for low-productivity, semi-arid ecosystems. The isolated effect of each environmental variable generally aligns with the results of the partial effect plots (Figure 5), with the exception of soil temperature. This is because we isolated the individual effect of soil temperature from the other variables and the partial effect analysis considered the combined effect of all the predictor variables that are held at average values. Results once again indicated that increasing soil water tension (more negative Ψ_{soil}) resulted in declines of productivity of vegetation. The threshold of steeper decline in productivity was observed around 400 kPa, similar to the effect observed in Figure 5.

Ψ_{soil} exhibited relatively minor response variability, as indicated by the width of the interquartile range (gray ribbon), compared to the other environmental variables (Figure 6). Optimal VPD conditions for plant productivity were again evident around 1kPa, with a general decline observed when drier atmospheric conditions occurred. In contrast to the partial effect analysis, when soil temperature is considered in isolation from the interactions of other environmental variables, our results indicate a slight negative effect on vegetation greenness associated with warmer temperatures. Among all the predictor variables, VPD and soil temperature demonstrated the largest ranges in their interquartile values, indicating that there is more variability and uncertainty in the isolated effect or that subsurface conditions are important when considering these environmental forcings (Figure 6). VWC had fluctuations, with divergent responses of vegetation greenness for changes in VWC, and also displayed greater variability in its interquartile range compared to Ψ_{soil} (Figure 6).

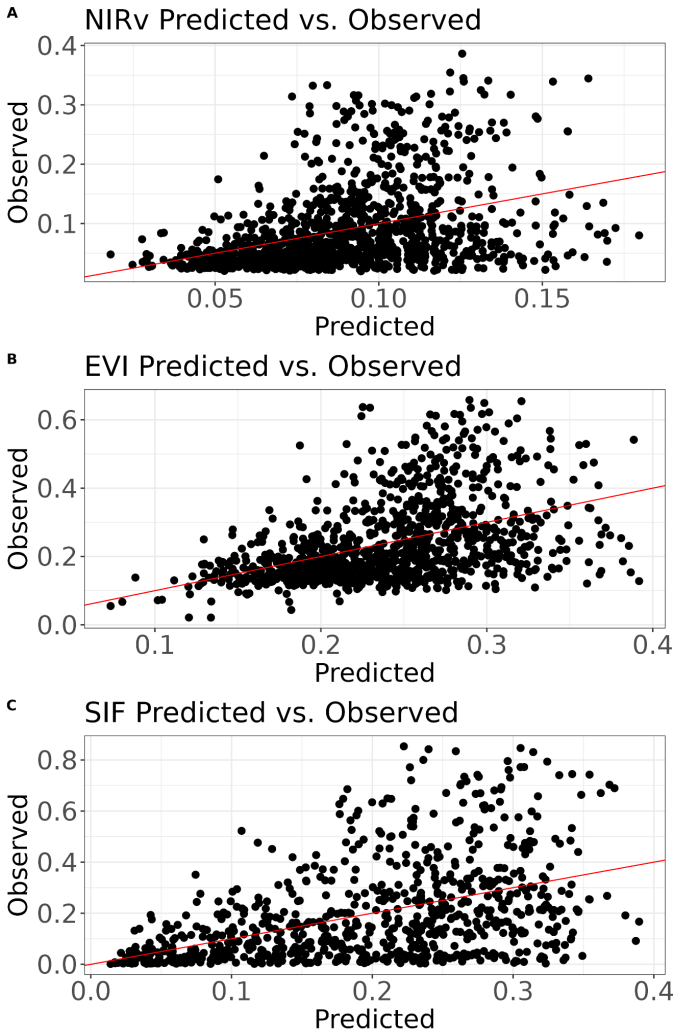

Figure 6. Comparison of observed and predicted values for the NIRv, EVI, and SIF GAM models. The red line is a 1 to 1 line.

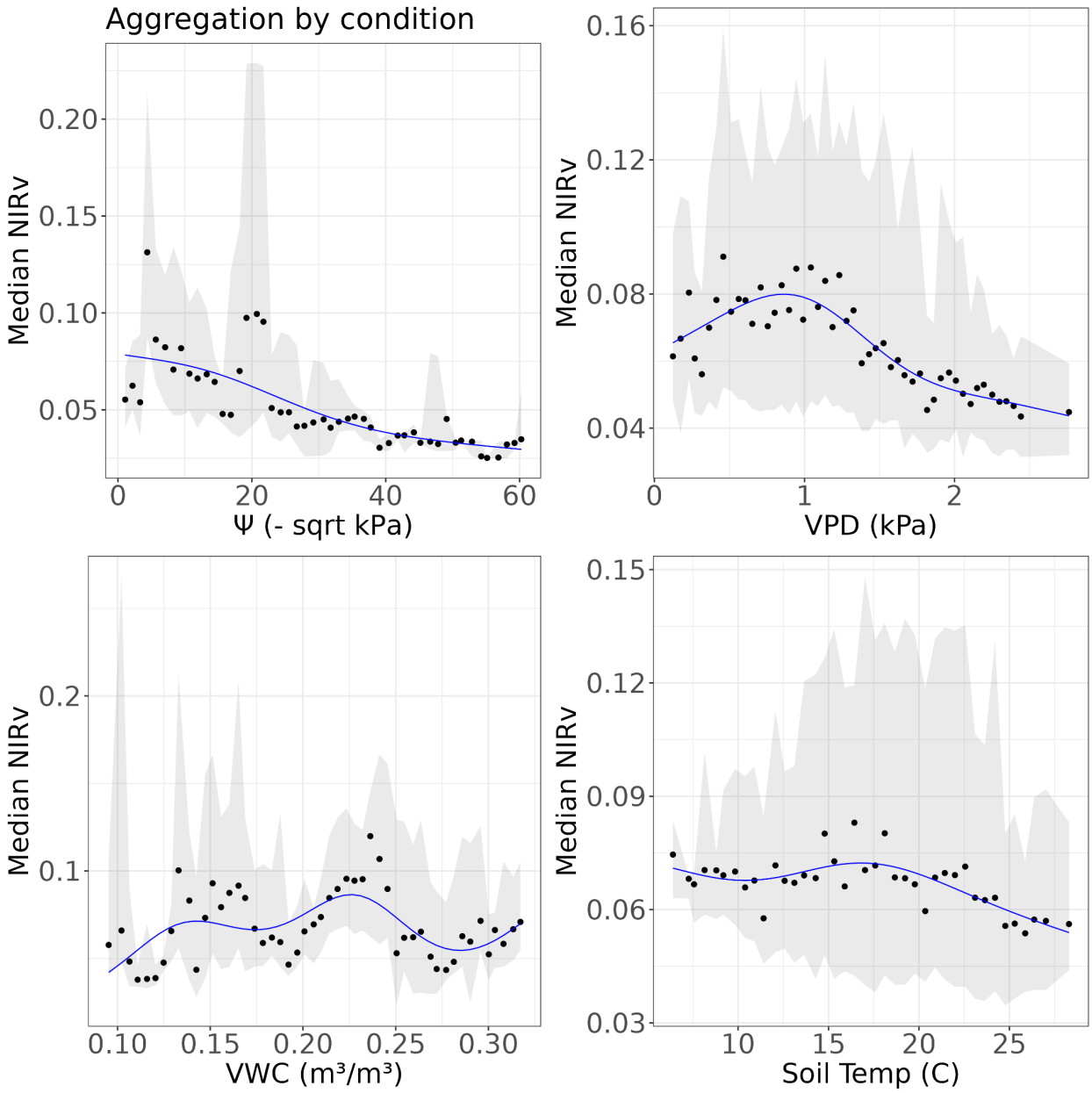

Figure 7. Plots illustrating the independent effects of Ψ_{soil}, VPD, VWC and soil temperature on NIRv.

3.3 Anomaly Analysis

We conducted an anomaly analysis in order to evaluate whether anomalies in Ψ_{soil}, VWC, VPD or soil temperature were most important for determining anomalies in vegetation greenness. However, following parametric normalization of these environmental variables, we found strong correlation between Ψ_{soil} and VWC (Figure 8). This result is ultimately intuitive because Ψ_{soil} are derived from VWC via the transformation function defined by the SWRC. Furthermore, the standardization procedure used

here accounts for non-normal data distributions, and therefore, accounts for differences in soil texture that is represented by Ψ_{soil}. Given the high correlation between these variables and the potential modeling issues associated with multicollinearity in GAMs (Afifi and Clark, 1996; Montgomery and Peck, 1992), VWC was excluded from the full GAM anomaly model. Ψ_{soil} was retained as the representative variable for subsurface conditions and included in the model along with VPD and soil temperature. We chose Ψ_{soil} over VWC because Ψ_{soil} had better model performance over VWC (Table 2 and Figure 5), although both variables are essentially interchangeable, and either variable would likely yield the same results.

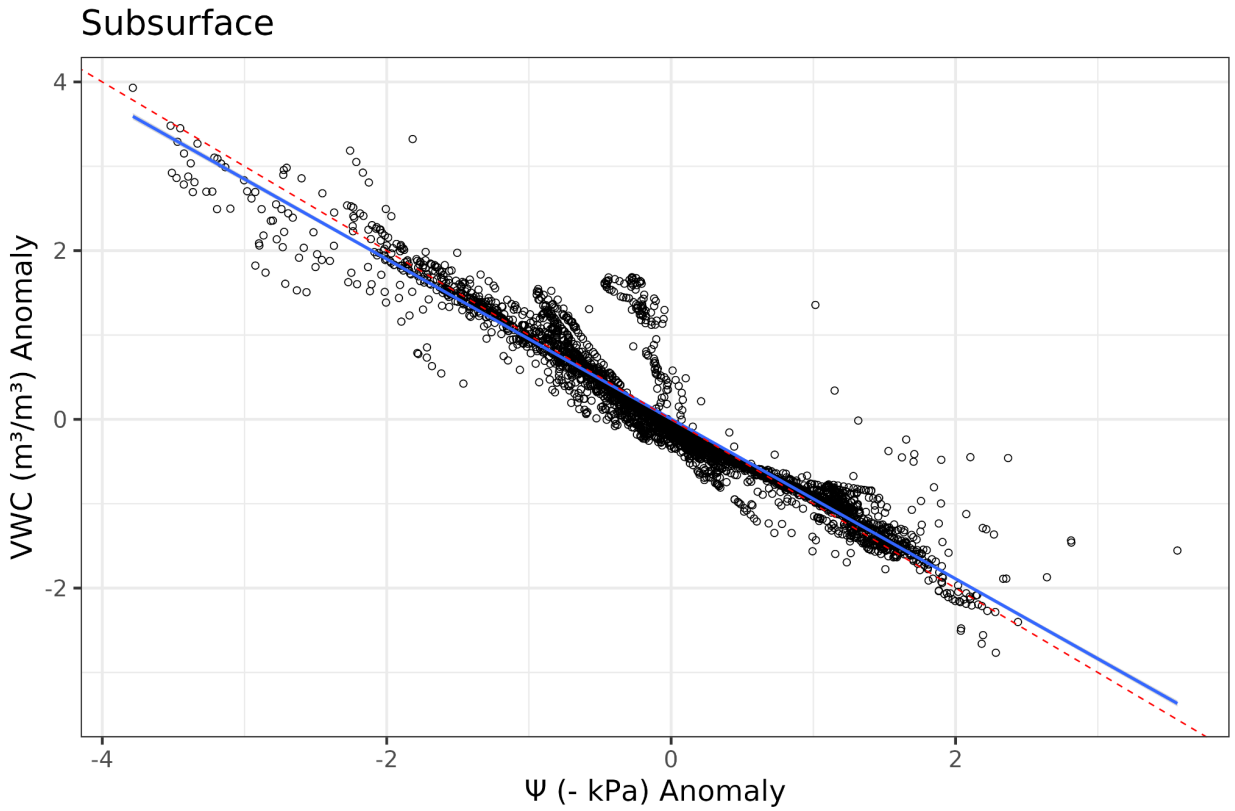

Figure 8. Scatterplot showing the relationship between parametrically standardized Ψ_{soil} and VWC variables in the anomaly analysis. The dashed red line represents a 1:1 linear relationship while the blue line is the linear relationship between Ψ_{soil} and VWC.

The deviance explained for the NIRv anomaly GAM model was 26.74% (Table 3). While all predictors had significant p-values, anomalies in subsurface conditions (Ψ_{soil}) was the only predictor found to have a significant PDC (Table 2). The negative PDC scores for VPD and soil temperature anomalies indicate that removing Ψ_{soil} anomalies from the model led to a deterioration in model performance. Figure 9 presents the partial effect plots for the NIRv anomaly GAM model. The Ψ_{soil} anomalies were more consistent overall than the VPD anomalies and soil temperature anomalies. The partial effects of Ψ_{soil} anomalies align with the observed trends in the seasonal and regional analyses, where anomalously dry subsurface conditions (Ψ_{soil} anomalies) resulted in anomalous declines in vegetation productivity responses. Overall, there was a general negative decline in vegetation productivity associated with increasing dryness from VPD anomalies. Very low (wet) VPD anomalies did result in a very slight increase in vegetation productivity. The effects of soil temperature anomalies were relatively

subtle, but consistently demonstrated a gradual increase in productivity anomalies, with a steeper incline towards warmer temperatures. Wetter VPD anomalies exhibited higher uncertainty and variability, while soil temperature anomalies displayed greater variability in drier conditions.

NIRv standardized anomaly GAM model, Deviance Explained = 26.74%

Variables	Partial Deviance Change	edf	Ref.df	F	p-value
Ψ (kPa) Anomaly	**600.41693**	**4.897951**	**4.995047**	**192.507069**	**0.0e+00**
VPD (kPa) Anomaly	-6.56947	4.080649	4.658369	20.288015	0.0e+00
Soil Temperature (C) Anomaly	-45.71509	4.649087	4.946934	6.373614	5.5e-06

Table 3. Overview of NIRv anomaly GAM model summary outputs and PDC for Ψ_{soil}, VPD and soil temperature anomalies.

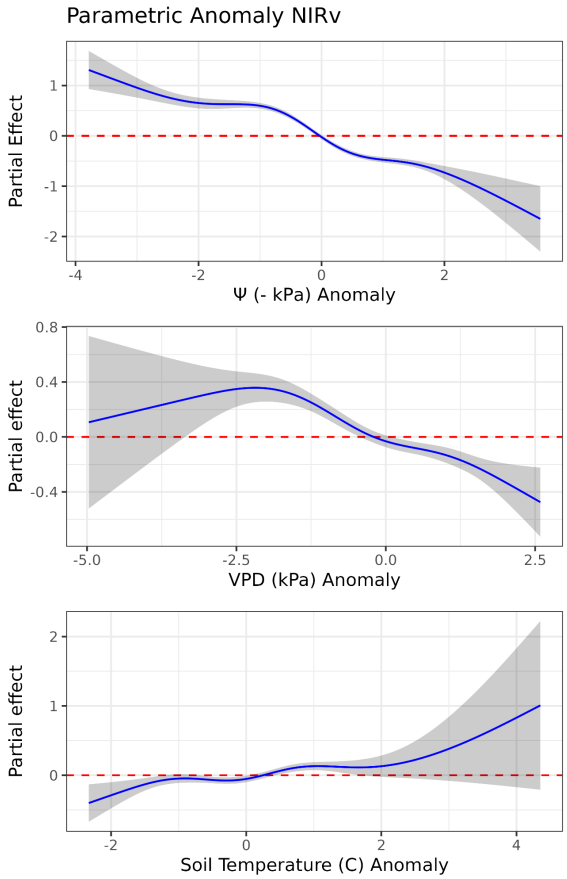

Figure 9. Partial effect plots depicting the relationship between NIRv and predictor variables in the standardized anomaly GAM model.

We evaluated how anomalies in environmental conditions related to anomalies in vegetation response for each environmental variable independently (Figure 10). To maintain consistency with the previous analysis, we employed GAMs to assess these anomaly relationships. However, standardization of the data resulted in a generally linear relationship. In light of this observed linear relationship, we also computed a linear model for each predictor variable in Figure 9. All predictor anomalies exhibited a negative relationship with NIRv, where drier or warmer than normal conditions typically resulted in brown vegetation anomalies. However, Ψ_{soil} anomalies displayed the strongest correlation, while VPD anomalies and soil temperature anomalies resulted in minor correlations.

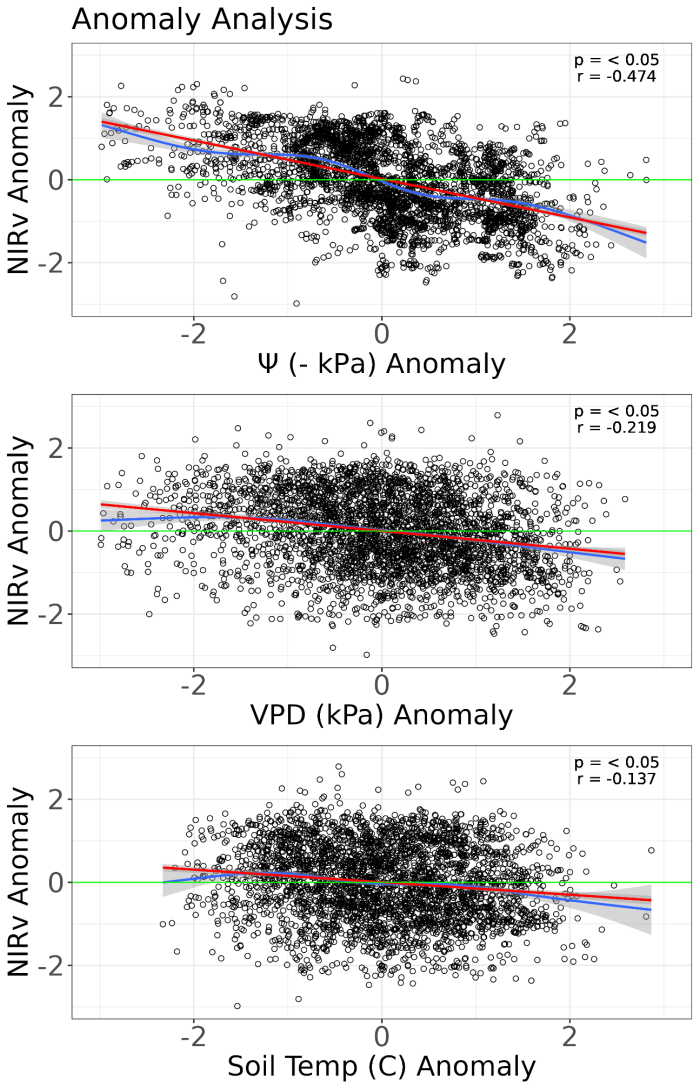

Figure 10. Scatter plot depicting the relationship between predictor anomalies and NIRv anomalies. The green line represents a flat line with no effect at y = 0, the blue line represents the NIRv GAM model, and the red line is a linear model.

4.0 Discussion

4.1 Seasonal analysis

Ψ_{soil} emerged as the dominant driver in explaining seasonal vegetation productivity across all models (Table 2 and Figure 5) when aggregating responses across sites in order to isolate the individual effects for each predictor variable. Furthermore, our analysis suggests that Ψ_{soil} was the most consistent driver explaining seasonal, regional and climatic anomaly patterns, confirming that absolute and relative increases in soil water tension (more negative Ψ_{soil}) are first order controls on vegetation declines (Figure 11). This key result is in agreement with a study conducted by Wilsk et al. (2010), which used eddy covariance flux data to conclude that Ψ_{soil} was the main driver regulating evapotranspiration fluxes for two semi-arid, shrub-dominated regions (Kubuqi Desert in China and the Sierra Madre mountain range in Wyoming, USA) when compared to VWC and VPD. Our analysis also highlights a threshold of Ψ_{soil} at approximately 400 kPa, both in the individual and interactive effects, which was associated with a decline in vegetation growth. This could be attributed to normal, seasonal phenological responses at the end of the growing season, but may also indicate a critical point where it becomes more difficult for plants to extract water effectively. This threshold is far lower than the threshold of 1500 kPa commonly indicated in the literature (Briggs and Shantz, 1912; Veihmeyer and Hendrickson, 1928; Kirkham, 2014) which originally came from work conducted on sunflowers (Briggs and Shantz, 1912). This suggests that the plant wilting point likely varies depending on species and that it isn't dependent on a single threshold value (Wiecheteck et al., 2020). Finally, we observed greater variability in the response of the other predictor variables (Figure 7), which reflect that the role of the other drivers are largely dependent on the conditions of Ψ_{soil}. As a whole, our results highlight that soil texture is very important in determining plant available water and subsequent vegetation stress, and the inclusion of Ψ_{soil} supports Novick et al's (2022) suggestion that disregarding soil properties obscures the importance of subsurface conditions.

In the absence of significant Ψ_{soil} limitations in semi-arid ecosystems, VPD emerges as a secondary driver for vegetation productivity (Figure 11). This is supported by the PDC score of the NIRv and SIF GAM model (in the EVI model, VWC was barely above VPD) (Table 2 and Figure 5). NIRv is considered a more representative index of vegetation productivity for semi-arid ecosystems (Wang et. al, 2022), which provides more confidence in our result that VPD is the 2nd limiting driver. Wilsk et al. (2010) also found that VPD becomes the primary limiting driver influencing evapotranspiration in semi-arid regions when Ψ_{soil} reaches low (wet) values. The seasonal analysis reveals that the general effect of increasing VPD on vegetation growth for semi-arid regions is negative (refer to the NIRv model in Figure 5), which supports findings from previous studies (Ridgen et al, 2020; Yu et al 2020); drier air is typically associated with a reduction in vegetation productivity. This may have important implications for irrigated regions, where VPD could be the dominant limiting driver for crops in wetter soils, and therefore, lower Ψ_{soil} tension (Ridgen et al., 2020). However, our seasonal analysis shows (Figures 5 and 7) that low VPD (about 1 kPa) may also enhance vegetation productivity, when Ψ_{soil} is not limiting, and below 1 kPa is too humid and hinders plant growth. Yu et al. (2022) found similar results in their research on dryland Central Asia; low to moderate VPD increased photosynthesis for croplands, grasslands and forests for moderate levels of VWC. However, Dubey and Gosh (2023) found that the positive effects of high VPD on plant growth are heterogeneous and are dependent on soil moisture. Alternatively, other studies have found that high VPD can enhance vegetation productivity in wetter regions (Cheng et al., 2022; Green et al., 2022), as increases in VPD allow for increased transpiration when subsurface moisture is abundant and Ψ_{soil} values are low (i.e. less negative) (Carins and Murphy et al., 2014; Inoue et al., 2021).

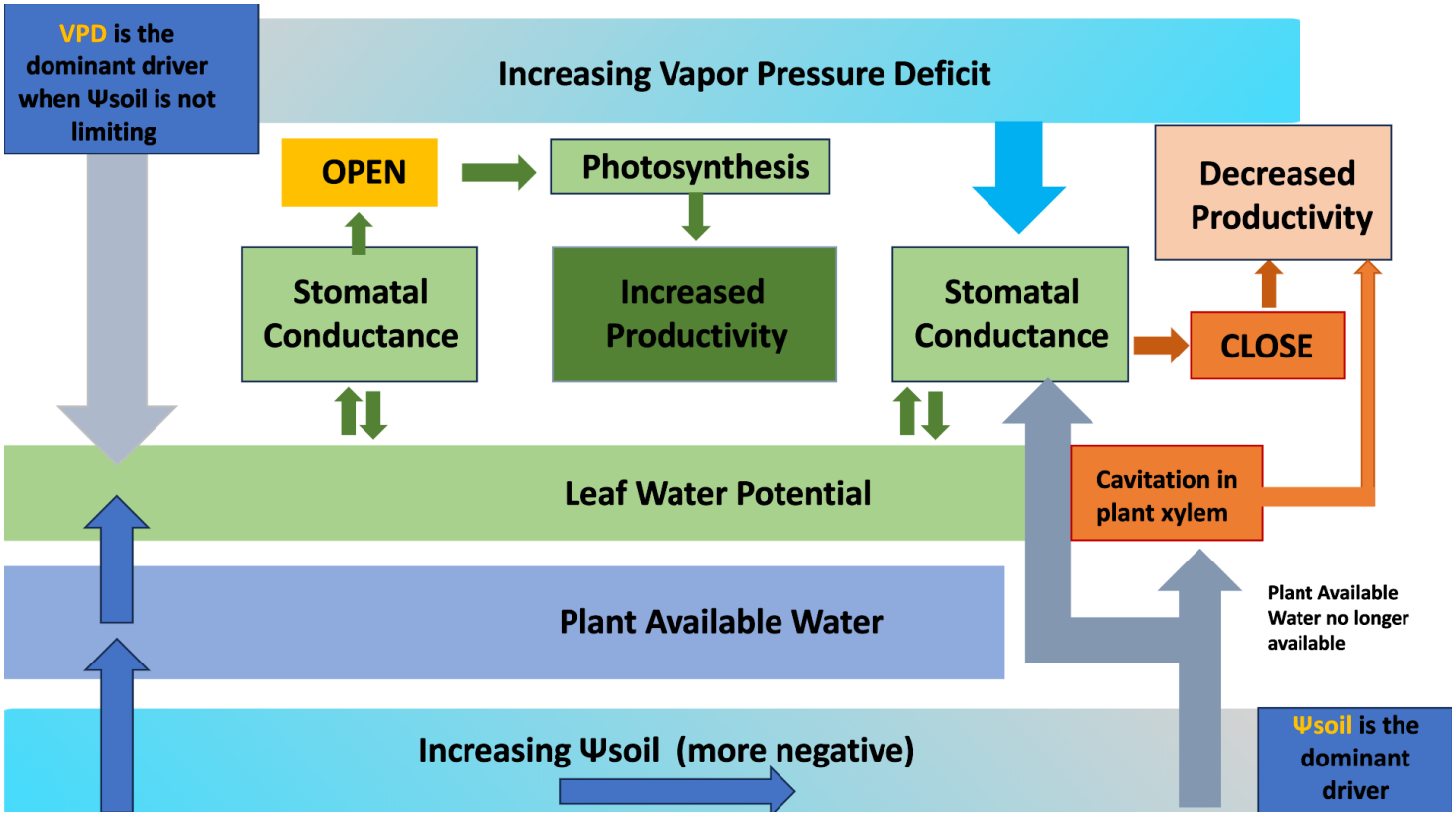

Figure 11. A conceptual diagram that shows how vegetation responds to changes in Ψ_{soil} and VPD. Ψ_{soil} is the dominant driver in explaining seasonal vegetation productivity for semi-arid ecosystems. Ψ_{soil} directly influences leaf water status, which controls important plant physiological mechanisms such as stomatal closure and xylem hydraulic processes. Early spring or precipitation events contribute to wetter subsurface conditions and low Ψ_{soil} tensions and allow for easier extraction of water from soil particles. When subsurface conditions are dry and Ψ_{soil} tensions are high, plants will no longer be able to extract water molecules that are tightly bound to soil particles. This can lead to stomatal closure or cause cavitation in the plant xylem. If Ψ_{soil} is not limiting, VPD becomes the dominant driver for vegetation productivity. Moderate increases of VPD can increase transpiration, and therefore, photosynthesis activity and plant growth. However, high VPD will negatively influence vegetation productivity by causing stomatal closure in an effort to save water loss.

The seasonal analysis revealed that soil temperature exerts little influence on vegetation productivity, relative to the other biophysical variables included in this analysis. This could be because this study was limited to the growing season (from May to September) and soil temperatures were already within an optimal range for growth (Gavito et al., 2001; Schwarz et al., 1997; Synman, 2002). Soil temperature had different effects in the independent analysis and the partial effect analysis, which is likely due to the influence of Ψ_{soil}. In the independent analysis for soil temperature, warmer soil temperatures led to slight decrease in vegetation productivity. In the partial effect analysis, when Ψ_{soil} is held at an average

value, soil conditions are wet enough that warmer temperatures led to moderate increases in vegetation productivity.

The irregular response of vegetation to VWC as seen in the seasonal analysis (Figure 5 and Figure 6), demonstrates inconsistent abiotic effects, implying that VWC alone does not fully capture the subsurface drivers influencing vegetation productivity. We hypothesize that the irregular responses of vegetation growth to VWC are related to differences in site specific soil properties, such as soil texture and hydraulic conductivity. This site specific response to VWC would in turn cause these observed irregularities when sites were aggregated across space in the seasonal analysis (e.g. absolute values of VWC impart differential impacts on plant stress depending on soil). Our results support previous studies that have found that plant available water is a function of both precipitation (here absolute values of soil moisture) and soil texture (Case and Staver 2018; Cook and Irwin, 1992; Hou et al 2021; O'Donnell and Ignizio 2012; Renee et al. 2019; Sala et al., 1997; Zhu et al 2022). For example, in semi-arid regions, Noy-Meir (1973) coined the "inverse texture hypothesis", which describes the phenomenon of plant growth favoring coarse-textured soils over fine-textured soils, due to its ability to allow infiltration to deeper soils and avoid evaporation loss. Sala et al (1988) observed that the inverse texture effect is dependent on annual precipitation and that the texture effect reverses in more humid regions. These studies highlight the influence of soil properties on plant growth and our results show that Ψ_{soil} can account for these differences in soil properties, making it a more precise biophysical indicator of vegetation water stress than VWC.

Our seasonal analysis revealed the inherent sensitivity of model results to the selection of parameters and methodology. If Ψ_{soil} had not been included in this analysis, the main limiting driver would have been highly dependent on the remotely sensed vegetation index chosen. This methodological dependency may be partially responsible for the debate in the literature regarding the dominant abiotic driver (VPD or VWC) of vegetation growth, in which many studies utilize different spectral indices, spatial and temporal resolutions, and models (Green et al., 2020; Novick et. al., 2016; Liu et al., 2020; Lu et al., 2022; Stocker et. al., 2018; Yao et al., 2023; Yu et al., 2022; Yuan et al., 2019). Furthermore, our study results suggest taking caution in the application of linear models to represent abiotic - vegetation relationships, as our findings confirm the highly nonlinear response of vegetation productivity to changing magnitudes of, and interactions between VWC, Ψ_{soil} ,VPD and soil temperature. We also highlight the challenges associated with identifying the primary drivers governing more productive vegetation, which may contribute to the lower deviance explained estimates observed in the GAM models (see Figure 6). Based on our conclusion that Ψ_{soil} is the main driver for vegetation productivity, the productive end typically occurs when Ψ_{soil} tension is low, resulting in other environmental factors driving vegetation productivity. We observed that VWC, VPD and soil temperature have more variability in their effect (Figure 6 and Figure 7), which likely contributes to the poor model performance at more productive sites or seasons. Therefore, our analysis cannot fully elucidate what drivers are responsible for variations in plant growth when plants are healthy and not stressed. This is likely associated with various interactions between these environmental drivers, or it may be reflecting other biotic and abiotic factors that were not included in this analysis, such as plant community physiological differences (Ackerly, 2004; Pivovaroff et al., 2016) or nutrient availability (Fernandez-Martinez et al., 2014). Several studies conducted at the regional scale have reported different climatic or environmental drivers of vegetation growth and productivity (Nemani et al 2003; Li et al 2017; Li et al 2022), which highlight inherent difficulty in disentangling these controls. However, the water stressed end of the vegetation indices

exhibited stronger predictive capabilities across all models, proving greater confidence in the model's ability to forecast vegetation response to prolonged periods of water stress.

4.2 Anomaly Analysis

An interesting, yet intuitive, finding of this study was the strong correlation between VWC anomalies and Ψ_{soil} anomalies at the site level - suggesting that VWC and Ψ_{soil} may be used interchangeably when characterizing vegetation water stress. We emphasize that this finding is only applicable for anomaly analysis that uses the same parametric standardization outlined in the methods section. This carries significant implications for future research that wishes to examine how relative environmental drivers (expressed as anomalies) of the soil and the atmosphere impact vegetation productivity, particularly in the context of using Ψ_{soil}. Our results show that the parametric standardization methods used here normalized the data and effectively account for differences in soil texture, obviating the need for Ψ_{soil} measurements when anomalies are the focus. This is because parametric anomalies at the site level implicitly account for soil texture via the statistical distributions that the specific VWC time series record. If capturing anomalies is the main objective, such as for drought early warning,VWC anomalies may serve as a suitable representation of subsurface conditions and relative plant water stress. However, our seasonal analysis underscored the importance of Ψ_{soil} as a dominant predictor for driving seasonal vegetation productivity when using absolute values (m^3/m^3 or Ψ). When examining absolute data at the seasonal scale, where the goal is to conduct a more precise and sensitive assessment, Ψ_{soil} should be incorporated into these types of studies to gain comprehensive insights.

Anomalies in subsurface moisture were identified as being the first order driver of vegetation anomalies in semi-arid regions (Table 2). This is in agreement with the previous research that assessed the influence of VWC and VPD for these ecosystems and found soil moisture as the dominant limiting factor (Xu et al. 2016; Yu et al; 2022). The variability observed for VPD anomalies and soil temperature anomalies (refer to Figure 9) likely reflect the influence of soil conditions on the responses of VPD and soil temperature. Meanwhile, the relationship between subsurface anomalies and vegetation anomalies is clear; wetter soil anomalies corresponded to increases in vegetation productivity anomalies, while dryer soil anomalies correspond to declines in vegetation productivity anomalies (Figure 10). In the context of drought impacts (which, by definition is an anomaly) our results suggest that subsurface conditions will have a greater influence on vegetation compared to atmospheric conditions. Drought monitoring efforts and climate models may want to focus on precipitation, the primary source of soil moisture (McColl et al 2017), and consider integrating subsurface moisture measurements into modeling endeavors for arid and semi-arid regions.

5.0 Conclusions

Our study represents an unprecedented evaluation of the effects of measured water potential on vegetation productivity in semi-arid regions, specifically focusing on rangeland ecosystems in Montana. By utilizing field-based, in-situ observations and incorporating Ψ_{soil} measurements into our analysis, we have contributed direct evidence that increase our understanding on the relative importance of VPD and subsurface soil conditions in determining vegetation productivity. We have shown that for semi-arid regions that are characterized by perennial forbs and grasses, Ψ_{soil} is the dominant hydrologic driver of seasonal vegetation productivity, and that increasing dryness (lower or more negative Ψ_{soil}) leads to declines in vegetation greenness. However, VPD appears to be a secondary driver of vegetation productivity in the absence of Ψ_{soil} limitations. Ψ_{soil} is able to capture the influence of soil structure on

plant available water more effectively than VWC, and therefore is a better predictor of vegetation stress. Finally, subsurface moisture anomalies were much more predictive of anomalies in vegetation greenness when compared to anomalies in atmospheric conditions. By bridging the research gap and emphasizing the importance of Ψ_{soil} in vegetation productivity for semi-arid regions, our study takes significant steps toward better understanding the mechanisms leading to water stress in vulnerable ecosystems. It is important to note that this study focused solely on semi-arid regions characterized by dominant perennial forbs and grasses. To gain comprehensive understanding of the role of Ψ_{soil}, VWC, and VPD as limiting drivers, future investigations may extend their scope to different vegetation types and ecosystems to assess whether the primary drivers remain consistent or exhibit variations depending on the specific ecological context. Furthermore, our study did not identify different soil types (i.e. sand vs. clay) and relate them to Ψ_{soil}. Quantifying Ψ_{soil} by soil type could help advance predictions and early warning systems for vegetation water stress in semi-arid landscapes and aid in spatial extrapolation.

6.0 Supplemental Information

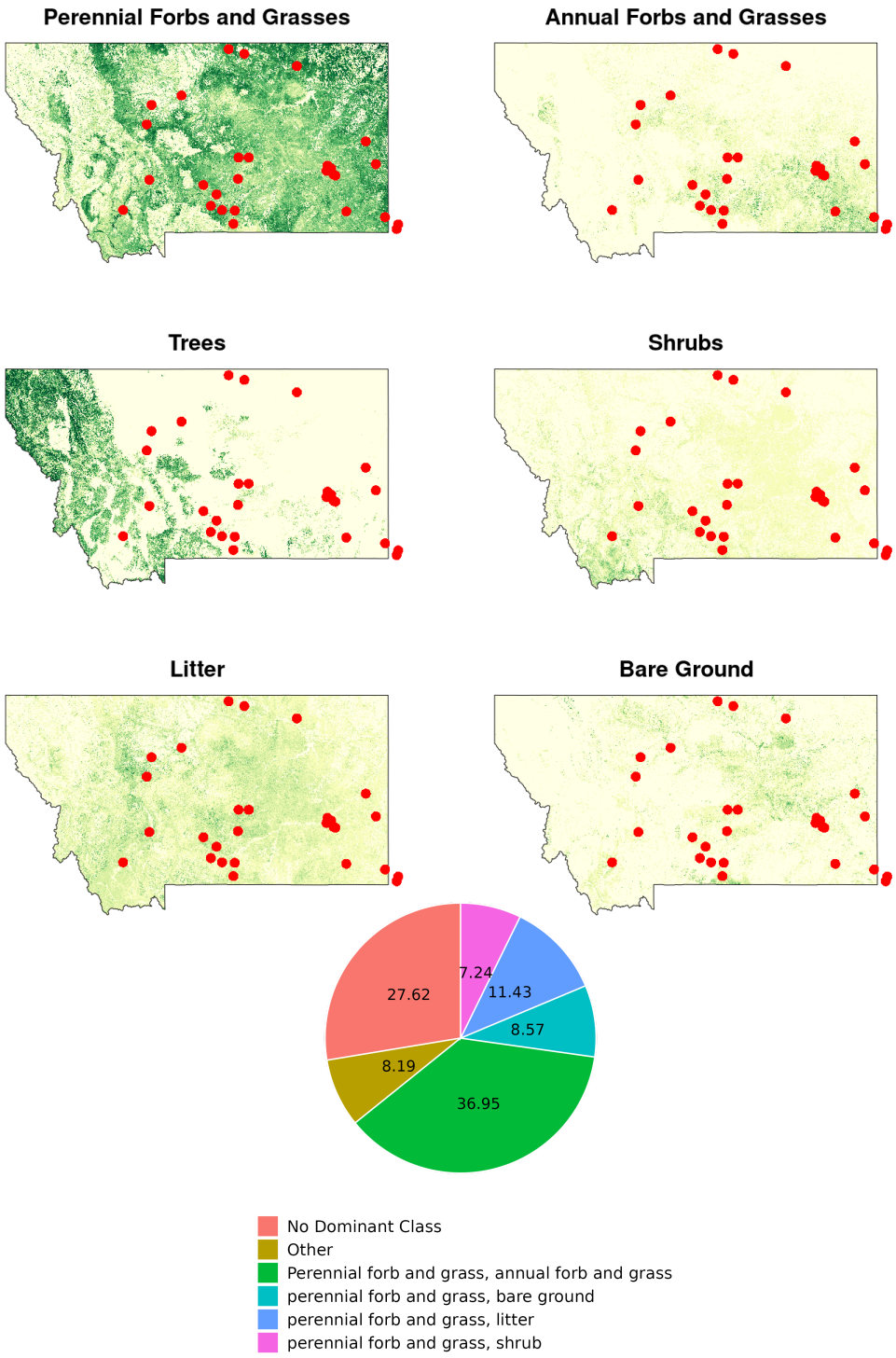

Figure S1. RAP 2022 estimates of vegetation cover for the state of Montana. The red circles are Mesonet site locations used in the seasonal analysis. Sites that contained "no dominant class" or "other" were excluded from the analysis.

7.0 References

Ackerly, D. (2004). Functional strategies of chaparral shrubs in relation to seasonal water deficit and disturbance. Ecological Monographs, 74(1), 25-44.

Afifi, A., May, S., & Clark, V. A. (2003). Computer-aided multivariate analysis. CRC Press.

Afshar, M. H., & Yilmaz, M. T. (2017). The added utility of nonlinear methods compared to linear methods in rescaling soil moisture products. Remote Sensing of Environment, 196, 224-237.

Ahlström, A., Raupach, M. R., Schurgers, G., Smith, B., Arneth, A., Jung, M., ... & Zeng, N. (2015). The dominant role of semi-arid ecosystems in the trend and variability of the land CO2 sink. Science, 348(6237), 895-899.

Allred, B. W., Bestelmeyer, B. T., Boyd, C. S., Brown, C., Davies, K. W., Duniway, M. C., & Uden, D. R. (2021). Improving Landsat predictions of rangeland fractional cover with multitask learning and uncertainty. Methods in Ecology and Evolution, 12(5), 841-849.

Badgley, G., Field, C. B., & Berry, J. A. (2017). Canopy near-infrared reflectance and terrestrial photosynthesis. Science advances, 3(3), e1602244.

Boyer, J. S. (1970). Differing sensitivity of photosynthesis to low leaf water potentials in corn and soybean. Plant physiology, 46(2), 236-239.

Briggs, L. J., & Shantz, H. L. (1912). The wilting coefficient for different plants: And its indirect determination (No. 230). US Government Printing Office.

Brooks, R. H. (1965). Hydraulic properties of porous media. Colorado State University.

Brunbjerg, A. K., Hale, J. D., Bates, A. J., Fowler, R. E., Rosenfeld, E. J., & Sadler, J. P. (2018). Can patterns of urban biodiversity be predicted using simple measures of green infrastructure?. Urban Forestry & Urban Greening, 32, 143-153.
Carins Murphy, M. R., Jordan, G. J., & Brodribb, T. J. (2014). Acclimation to humidity modifies the link between leaf size and the density of veins and stomata. Plant, Cell & Environment, 37(1), 124-131.

Cheng, Y., Liu, L., Cheng, L., Fa, K., Liu, X., Huo, Z., & Huang, G. (2022). A shift in the dominant role of atmospheric vapor pressure deficit and soil moisture on vegetation greening in China. Journal of Hydrology, 615, 128680.

Cornelis, W. M., Khlosi, M., Hartmann, R., Van Meirvenne, M., & De Vos, B. (2005). Comparison of unimodal analytical expressions for the soil‐water retention curve. *Soil Science Society of America Journal*, *69*(6), 1902-1911.

Daly, E., & Porporato, A. (2005). A review of soil moisture dynamics: from rainfall infiltration to ecosystem response. Environmental engineering science, 22(1), 9-24

Dubey, N., & Ghosh, S. (2023). The relative role of soil moisture and vapor pressure deficit in affecting the Indian vegetation productivity. Environmental Research Letters, 18(6), 064012.

Elzhov, T. V., Mullen, K. M., Spiess, A., & Bolker, B. (2010). R interface to the Levenberg-Marquardt nonlinear least-squares algorithm found in MINPACK. Plus support for bounds, 1-2.

Fernández-Martínez, M., Vicca, S., Janssens, I. A., Sardans, J., Luyssaert, S., Campioli, M., ... & Peñuelas, J. (2014). Nutrient availability as the key regulator of global forest carbon balance. Nature Climate Change, 4(6), 471-476.

Fredlund, D. G., & Xing, A. (1994). Equations for the soil-water characteristic curve. *Canadian geotechnical journal*, *31*(4), 521-532.

Fuentes, C., Haverkamp, R., & Parlange, J. Y. (1992). Parameter constraints on soil water characteristics. Indirect Methods for Estimating the Hydraulic Properties of Unsaturated Soils, 161-168.

Gavito, M. E., Curtis, P. S., Mikkelsen, T. N., & Jakobsen, I. (2001). Interactive effects of soil temperature, atmospheric carbon dioxide and soil N on root development, biomass and nutrient uptake of winter wheat during vegetative growth. Journal of experimental botany, 52(362), 1913-1923.

Ghanbarian-Alavijeh, B., Liaghat, A., Huang, G. H., & Van Genuchten, M. T. (2010). Estimation of the van Genuchten soil water retention properties from soil textural data. Pedosphere, 20(4), 456-465.

Gorelick, N., Hancher, M., Dixon, M., Ilyushchenko, S., Thau, D., & Moore, R. (2017). Google Earth Engine: Planetary-scale geospatial analysis for everyone. Remote sensing of Environment, 202, 18-27.

Green, J. K., Berry, J., Ciais, P., Zhang, Y., & Gentine, P. (2020). Amazon rainforest photosynthesis increases in response to atmospheric dryness. Science Advances, 6(47), eabb7232.

Hillel, D. (2003). Introduction to environmental soil physics. Elsevier.

Hu, J., Jia, J., Ma, Y., Liu, L., & Yu, H. (2022). A Reconstructed Global Daily Seamless SIF Product at 0.05 Degree Resolution Based on TROPOMI, MODIS and ERA5 Data. Remote Sensing, 14(6), 1504.

Huete, A., Justice, C., & Van Leeuwen, W. (1999). MODIS vegetation index (MOD13). *Algorithm theoretical basis document*, *3*(213), 295-309.

Inoue, T., Sunaga, M., Ito, M., Yuchen, Q., Matsushima, Y., Sakoda, K., & Yamori, W. (2021). Minimizing VPD fluctuations maintains higher stomatal conductance and photosynthesis, resulting in improvement of plant growth in lettuce. Frontiers in plant science, 12, 646144.

Jarvis, P. (1976). The interpretation of the variations in leaf water potential and stomatal conductance found in canopies in the field. Philosophical Transactions of the Royal Society of London. B, Biological Sciences, 273(927), 593-610.

Jiaochan Hu, & Liangyun Liu. (2022). A Reconstructed Global Daily Seamless TROPOMI SIF dataset at a 0.05-degree Resolution (SDSIF) using the ML approach [Data set]. Zenodo. https://doi.org/10.5281/zenodo.5888283

Jones, M. O., Allred, B. W., Naugle, D. E., Maestas, J. D., Donnelly, P., Metz, L. J., ... & McIver, J. D. (2018). Innovation in rangeland monitoring: annual, 30 m, plant functional type percent cover maps for US rangelands, 1984–2017. Ecosphere, 9(9), e02430.

Kaspar, T. C., & Bland, W. L. (1992). Soil temperature and root growth. Soil Science, 154(4), 290-299.

Katul, G. G., Oren, R., Manzoni, S., Higgins, C., & Parlange, M. B. (2012). Evapotranspiration: a process driving mass transport and energy exchange in the soil‐plant‐atmosphere‐climate system. Reviews of Geophysics, 50(3).

Kirkham, M. B. (2014). Principles of soil and plant water relations. Academic Press.

Kosugi, K. (1999). General model for unsaturated hydraulic conductivity for soils with lognormal pore‐size distribution. *Soil Science Society of America Journal*, *63*(2), 270-277.

Leong, E. C., & Rahardjo, H. (1997). Review of soil-water characteristic curve equations. *Journal of geotechnical and geoenvironmental engineering*, *123*(12), 1106-1117.

Levenberg, K. (1944). A method for the solution of certain non-linear problems in least squares. Quarterly of applied mathematics, 2(2), 164-168.

Li, L., Zeng, Z., Zhang, G., Duan, K., Liu, B., & Cai, X. (2022). Exploring the Individualized Effect of Climatic Drivers on MODIS Net Primary Productivity through an Explainable Machine Learning Framework. Remote Sensing, 14(17), 4401.

Li, P., Peng, C., Wang, M., Li, W., Zhao, P., Wang, K., ... & Zhu, Q. (2017). Quantification of the response of global terrestrial net primary production to multifactor global change. Ecological Indicators, 76, 245-255.

Lian, X., Piao, S., Chen, A., Huntingford, C., Fu, B., Li, L. Z., ... & Roderick, M. L. (2021). Multifaceted characteristics of dryland aridity changes in a warming world. Nature Reviews Earth & Environment, 2(4), 232-250.

Liu, L., Gudmundsson, L., Hauser, M., Qin, D., Li, S., & Seneviratne, S. I. (2020). Soil moisture dominates dryness stress on ecosystem production globally. Nature communications, 11(1), 4892.

Liu, L., Peng, S., AghaKouchak, A., Huang, Y., Li, Y., Qin, D., ... & Li, S. (2018). Broad consistency between satellite and vegetation model estimates of net primary productivity across global and regional scales. Journal of Geophysical Research: Biogeosciences, 123(12), 3603-3616.

Lyons, D. S., Dobrowski, S. Z., Holden, Z. A., Maneta, M. P., & Sala, A. (2021). Soil moisture variation drives canopy water content dynamics across the western US. Remote Sensing of Environment, 253, 112233.

Ma, X., Huete, A., Moran, S., Ponce‐Campos, G., & Eamus, D. (2015). Abrupt shifts in phenology and vegetation productivity under climate extremes. Journal of Geophysical Research: Biogeosciences, 120(10), 2036-2052.

Marquardt, D. W. (1963). An algorithm for least-squares estimation of nonlinear parameters. Journal of the society for Industrial and Applied Mathematics, 11(2), 431-441.

McColl, K. A., Alemohammad, S. H., Akbar, R., Konings, A. G., Yueh, S., & Entekhabi, D. (2017). The global distribution and dynamics of surface soil moisture. Nature Geoscience, 10(2), 100-104.

METER. (2019, November 18). METER; METER. https://www.metergroup.com/

Montgomery, D. C., Peck, E. A., & Vining, G. G. (2021). Introduction to linear regression analysis. John Wiley & Sons.

Nemani, R. R., Keeling, C. D., Hashimoto, H., Jolly, W. M., Piper, S. C., Tucker, C. J., ... & Running, S. W. (2003). Climate-driven increases in global terrestrial net primary production from 1982 to 1999. science, 300(5625), 1560-1563.

Oddi, F. J., Miguez, F. E., Ghermandi, L., Bianchi, L. O., & Garibaldi, L. A. (2019). A nonlinear mixed‐effects modeling approach for ecological data: Using temporal dynamics of vegetation moisture as an example. Ecology and evolution, 9(18), 10225-10240.

Pivovaroff, A. L., Pasquini, S. C., De Guzman, M. E., Alstad, K. P., Stemke, J. S., & Santiago, L. S. (2016). Multiple strategies for drought survival among woody plant species. *Functional Ecology*, *30*(4), 517-526.

Porporato, A., D'odorico, P., Laio, F., Ridolfi, L., & Rodriguez-Iturbe, I. (2002). Ecohydrology of water-controlled ecosystems. Advances in Water Resources, 25(8-12), 1335-1348.

Poulter, B., Frank, D., Ciais, P., Myneni, R. B., Andela, N., Bi, J., ... & van der Werf, G. R. (2014). Contribution of semi-arid ecosystems to interannual variability of the global carbon cycle. Nature, 509(7502), 600-603.

R Core Team (2020). R: A language and environment for statistical computing. R Foundation for Statistical Computing, Vienna, Austria. URL https://www.R-project.org/.

Renne, R. R., Bradford, J. B., Burke, I. C., & Lauenroth, W. K. (2019). Soil texture and precipitation seasonality influence plant community structure in North American temperate shrub steppe. Ecology, 100(11), e02824.

Restaino, C. M., Peterson, D. L., & Littell, J. (2016). Increased water deficit decreases Douglas fir growth throughout western US forests. Proceedings of the National academy of Sciences, 113(34), 9557-9562.

Russo, D., Bresler, E., Shani, U., & Parker, J. C. (1991). Analyses of infiltration events in relation to determining soil hydraulic properties by inverse problem methodology. Water Resources Research, 27(6), 1361-1373.

Sala, O. E., Parton, W. J., Joyce, L. A., & Lauenroth, W. K. (1988). Primary production of the central grassland region of the United States. Ecology, 69(1), 40-45.

Sala, O. E., W. K. Lauenroth, and R. A. Golluscio. 1997. Plant functional types in temperate semiarid regions. Pages 217–233 in T. M. Smith et al., editors. Plant functional types: their relevance to ecosystem properties and global change. Cambridge University Press, Cambridge, UK.

Schenk, H. J., & Jackson, R. B. (2002). Rooting depths, lateral root spreads and below-ground/above-ground allometries of plants in water-limited ecosystems. Journal of Ecology, 480-494.

Schwarz, P. A., Fahey, T. J., & Dawson, T. E. (1997). Seasonal air and soil temperature effects on photosynthesis in red spruce (Picea rubens) saplings. Tree physiology, 17(3), 187-194.

Soto, M. A., Chang, H. K., & Van Genuchten, M. T. (2017). Fractal-based models for the unsaturated soil hydraulic functions. Geoderma, 306, 144-151.

Sperry, J. S., Hacke, U. G., Oren, R., & Comstock, J. P. (2002). Water deficits and hydraulic limits to leaf water supply. Plant, cell & environment, 25(2), 251-263.

Sperry, J. S., Stiller, V., & Hacke, U. G. (2003). Xylem hydraulics and the soil–plant–atmosphere continuum: opportunities and unresolved issues. Agronomy Journal, 95(6), 1362-1370.

Stankovich, J. M., & Lockington, D. A. (1995). Brooks-Corey and van Genuchten soil-water-retention models. Journal of Irrigation and drainage Engineering, 121(1), 1-7.

Stocker, B. D., Zscheischler, J., Keenan, T. F., Prentice, I. C., Peñuelas, J., & Seneviratne, S. I. (2018). Quantifying soil moisture impacts on light use efficiency across biomes. New Phytologist, 218(4), 1430-1449.

Too, V. K., Omuto, C. T., Biamah, E. K., & Obiero, J. P. (2014). Review of soil water retention characteristic (SWRC) models between saturation and oven dryness. Open Journal of Modern Hydrology, 4(04), 173.

Too, V., Omuto, C. T., Biamah, E. K., & Obiero, J. P. (2021). PERFORMANCE EVALUATION OF THE POPULAR SWRC MODELS AT DIFFERENT SOIL BULK DENSITY RANGES.

Van Genuchten, M. T. (1980). A closed‐form equation for predicting the hydraulic conductivity of unsaturated soils. *Soil science society of America journal*, *44*(5), 892-898.

Veihmeyer, F. J., & Hendrickson, A. H. (1928). Soil moisture at permanent wilting of plants. Plant Physiology, 3(3), 355.

Wang, X., Biederman, J. A., Knowles, J. F., Scott, R. L., Turner, A. J., Dannenberg, M. P., ... & Smith, W. K. (2022). Satellite solar-induced chlorophyll fluorescence and near-infrared reflectance capture complementary aspects of dryland vegetation productivity dynamics. Remote Sensing of Environment, 270, 112858.

Wiecheteck, L. H., Giarola, N. F., de Lima, R. P., Tormena, C. A., Torres, L. C., & de Paula, A. L. (2020). Comparing the classical permanent wilting point concept of soil (− 15,000 hPa) to biological wilting of wheat and barley plants under contrasting soil textures. Agricultural Water Management, 230, 105965.

Wilske B., Kwon H., Wei L., et al. (2010) Evapotranspiration (ET) and regulating mechanisms in two semiarid Artemisia-dominated shrub steppes at opposite sides of the globe. J Arid Environ 74: 1461–70.

Wood, S. (2012). mgcv: Mixed GAM Computation Vehicle with GCV/AIC/REML smoothness estimation.

Wösten, J. H. M., Pachepsky, Y. A., & Rawls, W. J. (2001). Pedotransfer functions: bridging the gap between available basic soil data and missing soil hydraulic characteristics. Journal of hydrology, 251(3-4), 123-150.

Wu, Z., Bi, J., & Gao, Y. (2021). Drivers and environmental impacts of vegetation greening in a semi-arid region of northwest China since 2000. Remote Sensing, 13(21), 4246.

Xu, Chonggang & McDowell, Nate & Rosie, Fisher & Wei, Liang & Sevanto, Sanna & Christoffersen, Bradley & Weng, Ensheng & Middleton, Richard. (2019). Increasing impacts of extreme droughts on vegetation productivity under climate change. Nature Climate Change. 9. 10.1038/s41558-019-0630-6.

Xu, H. J., Wang, X. P., & Zhang, X. X. (2016). Decreased vegetation growth in response to summer drought in Central Asia from 2000 to 2012. International journal of applied earth observation and geoinformation, 52, 390-402.

Yao, Y., Liu, Y., Zhou, S., Song, J., & Fu, B. (2023). Soil moisture determines the recovery time of ecosystems from drought. Global Change Biology.

Yu, T., Jiapaer, G., Bao, A., Zheng, G., Zhang, J., Li, X., ... & Umuhoza, J. (2022). Disentangling the relative effects of soil moisture and vapor pressure deficit on photosynthesis in dryland Central Asia. Ecological Indicators, 137, 108698.

Yuan, W., Zheng, Y., Piao, S., Ciais, P., Lombardozzi, D., Wang, Y., ... & Yang, S. (2019). Increased atmospheric vapor pressure deficit reduces global vegetation growth. Science advances, 5(8), eaax1396.

Zheng, W., Shen, C., Wang, L. P., & Jin, Y. (2020). An empirical soil water retention model based on probability laws for pore‐size distribution. *Vadose Zone Journal*, *19*(1), e20065.

Zhou, S., Williams, A. P., Berg, A. M., Cook, B. I., Zhang, Y., Hagemann, S., ... & Gentine, P. (2019). Land–atmosphere feedbacks exacerbate concurrent soil drought and atmospheric aridity. Proceedings of the National Academy of Sciences, 116(38), 18848-18853.

Zhu, X., Liu, H., Xu, C., Wu, L., Shi, L., & Liu, F. (2022). Soil coarsening alleviates precipitation constraint on vegetation growth in global drylands. Environmental Research Letters, 17(11), 114008.